2026 IEEE International Conference on Robotics and Automation (ICRA 2026)
June 1-5, 2026. Vienna, Austria

SPARO: Snap-On/Rotate-Off Passive Gripper for Aerial Perching

Jakob Domislovic, Antun Ivanovic, Frano Petric and Matko Orsag

***Abstract*— We present SPARO, a fully passive, impact-activated SnaP-on And Rotate-Off gripper for aerial perching that requires no onboard actuation or sensing for closing or opening. SPARO is 3D-printed from PET-G, weighs 290 g, and closes upon impact within 45 ms using a bistable spring mechanism that can grasp objects up to 15 cm in diameter. The gripper opens through a mechanically coupled yaw motion from the host robot, enabling repeated autonomous perching without any additional actuation. A trajectory optimization framework based on nonlinear programming generates gripper-aware, full-state trajectories in SE(3) that promote approach from underneath the target and satisfy closure constraints. Extensive experiments confirm reliable, repeatable autonomous perching on various surfaces and robots, using off-the-shelf quadrotors, thus validating the system's simplicity, universality, and reproducibility.**

Keywords: passive gripper, aerial perching, trajectory

I. Introduction

Despite the rapid growth and widespread adoption of quadrotors, endurance remains fundamentally constrained by battery capacity and the high energetic cost of hover, which consumes the most power [1]. This limitation becomes critical in missions that require extended monitoring and sampling under strict safety and access constraints [2], [3]. A particularly relevant use case is CBRNE (chemical, biological, radiological, nuclear, and explosive) response, where communication may be lost, human access is hazardous, and robotic systems must operate autonomously over prolonged time. To meet these demands, we focus on an aerial perching framework that conserves energy by allowing the vehicle to attach to anchor points in the environment during dwell phases, while maintaining system simplicity and operational robustness.

Aerial perching poses three core challenges: (i) selection of a suitable perching location, (ii) designing an attachment mechanism that holds the robot with minimal or zero holding power, and (iii) planning and execution of the approach under dynamical and environmental constraints. This paper focuses on the latter two and builds on recent advances in trajectory generation for perching and passive gripper design.

This work was supported in part by the project "CBRNe HERO" funded by the European Union - NextGeneration EU under Grant NPOO.C3.2.R3-I1.04.0075. The work of doctoral student Jakob Domislovic has been supported in part by the "Young researchers' career development project–training of doctoral students" of the Croatian Science Foundation funded by the European Union from the European Social Fund.

All authors are with the University of Zagreb Faculty of Electrical Engineering and Computing, Zagreb 10000, Croatia jakob.domislovic at fer.unizg.hr

Fig. 1: Perching with SPARO on a tree branch.

A. Motivation

This work targets a universal perching solution that is low-cost, lightweight, fast, robust, and easily deployable. Well-suited to CBRNE-like missions where reliability and simplicity are essential. Many existing aerial perching systems require custom-built platforms, additional actuators, or dedicated sensing, limiting their versatility and reproducibility. In contrast, we propose a fully passive gripper that exploits the host robot's inherent actuation and sensing, already needed for flight, to enable repeated perching through body motion alone. No extra motors, electronics, or communication are required on the gripper, thus reducing the weight and power draw.

Trajectory generation is tightly coupled with the mechanism's passive dynamics, ensuring proper contact velocity and geometry for reliable engagement and repeatable perching. The goal is a minimal-complexity system that integrates seamlessly with standard and off-the-shelf quadrotors, making passive perching accessible and repeatable using only onboard tools. The example of successful perching with our proposed method is shown in Fig. 1.

B. Related work

Perching and grasping have been widely studied through the co-design of mechanical end-effectors and trajectory strategies. We group the related work accordingly and emphasize passive mechanisms that reduce control burden at contact, providing a comparison of representative aerial perching grippers against SPARO with Table I.

In [4], [5], the authors demonstrate compliant, mechanically intelligent grippers where impact-triggered state switching eliminates precise contact timing and enables energy-free holding. Beyond fast closure, these

TABLE I: Comparison of aerial perching grippers within the scope of this work. Opening and closing columns report what kind of actuation or sensing is used for that action. A dash '-' indicates that the value is not reported.

Property	[4]	[5]	[6]	[7]	[8]	[9]	[10]	[11]	[12]	[13]	[14]	**SPARO**
Weight [g]	28	40	22.7	322	551	150	-	400	700	142	37.8	290
Closure time [ms]	-	200	12	35	96	65	-	-	25	67	-	44
Payload [kg]	3.70	-	-	0.34	5.70	4.00	0.24	-	0.7	2.24	1.04	6
Closure force [N]	-	-	4.80	4.40	56	40.0	-	11.5	56.8	22	10.22	7
Activation force [N]	2.53	2.15	1.5	-	-	-	-	-	11.4	22.4	-	9
Grasp diameter [cm]	5.68	33.00	2.00	8.00	4.80	5.00	-	11.00	11.00	11.00	9.80	15
Closing	Passive	Passive	Passive	US sensor	IR sensor	Passive	Motor	Passive	Passive	Passive	Passive	Passive
Opening	Passive	Servo	Human	Servo	Servo	-	Motor	Passive	Servo	Servo	Servo	Passive

works are notable for low end-effector mass and passive holding without power, making them attractive when vehicle payload is limited. For ultra-light aerial platforms, the authors in [6] report a gripper in the tens-of-grams class, together with velocity sufficiency regions that link required contact forces to admissible approach velocities. Importantly, the design maintains a low mass while achieving repeatable capture of lightweight targets. The method in [7] utilizes an ultrasonic trigger and quick-release elastic latch, trading modest mass for sensing simplicity while retaining a compact form factor. Complementarily, the tendon-driven passive hand in [8] prioritizes grasp force via stored elastic energy at moderate end-effector mass, and [9] adds an electroadhesive clutch to self-lock tendons, increasing holding force without continuous power.

Soft and underactuated approaches broaden geometry tolerance. The fin-ray concept in [10] passively conforms to object shape with gentle contact, but it uses a motor for both closing and opening. The underactuated fingers in [11] adapt to rods, plates, and cones, with effective holding governed by vehicle weight and contact geometry. Both [10], [11] present interesting methods using soft grippers, however, for our case, the focus was more on rigid fingers. One such capability of passive actuation is described in [15], where a gripper is used for rough and irregular surfaces, microspines with preload, as described in [15], passively interlock with asperities and provide clamp-style force amplification. They tolerate misalignment (e.g., $\pm 30^\circ$) and use a low-power release, yielding high specific holding force (force per gripper mass) on bark/rock. Beyond multirotors, the flapping-wing system in [12] achieves autonomous perching using a low-mass, passively latching claw. The payload is limited but sufficient for platform self-weight support during perch. For long-duration tasks, the tether-entangling approach in [16] shifts load to the anchor via tension, minimizing onboard power during the attached phase. Where precise alignment is difficult, crash-perching methods in [13], [17], [18] use wing-mediated hugging of cylinders, emphasizing robustness over precision. Finally, the snap-through grippers in [14] exhibit multi-functionality (grip, jump, land) with high elastic energy return and holding forces on the order of tens of newtons relative to a lightweight structure.

In [19], the authors develop computationally efficient polynomial motion primitives that compress the online search over dynamically feasible segments for time-critical approaches. The trajectory generator MINCO [20] enforces geometric and state–input constraints to enable aggressive yet feasible SE(3) approach arcs in clutter, supporting precise endgame shaping without saturating actuators. Studies in [21], [22] show how lightweight mechanisms paired with trajectory shaping and perception expand viable landing attitudes and surface sets. Real-time planners in [23]–[25] utilize nonlinear optimization and onboard perception to perch on inclined or moving targets with fast replanning while maintaining visibility and collision constraints. Within this picture, the velocity sufficiency analysis of [6] provides a direct bridge from mechanism capabilities (mass, holding force, closure dynamics) to trajectory envelopes, ensuring approach conditions fall inside the passive closure and sustained-hold window.

To our knowledge, no prior work integrates a fully passive gripper, where both closure and opening are achieved without onboard actuation or sensing, with trajectory planning into a unified system for repeated aerial perching. SPARO combines impact-triggered closure and rotation-based opening in a bistable design, coupled with gripper-aware trajectory optimization. Unlike previous fully passive systems [4], [11], SPARO supports higher payloads, tolerates imprecise contacts, and has been validated across diverse surfaces and off-the-shelf quadrotors. Most existing designs rely on custom-built platforms or tight integration. In contrast, SPARO is actuator-free, lightweight, and mountable on any robot capable of body rotation, making it simple, robust, and widely deployable. While some NLP optimization [23] leverages powerful offboard computation for real-time replanning, our NLP runs entirely onboard with limited CPU resources and focuses on fixed perching points. Since we are not pursuing moving targets, but rather ensuring reliable attachment to static perching locations, the planning time remains acceptable, as speed is not the primary objective of this work.

C. Contributions and paper outline

The contributions of this work are:

- SPARO: the fully passive, low-cost, fast, and universal gripper that closes on contact by snapping and is reopened by rotation of the robot, enabling

repeatable perching without end-effector actuation, sensing, or human interaction, and straightforward integration on any robot.
- Holistic nonlinear program (NLP) that optimizes full-state trajectories in the gripper's coordinate frame, with shaping costs that bias the approach from below the anchor point. The planner is gripper-aware, incorporating positional constraints and mechanical considerations of the passive closure mechanism.
- Extensive experimental validation on multiple off-the-shelf robots with different gripper mounting positions, demonstrating the universality of the gripper and repeatable perching on diverse surfaces.

The paper is organized as follows. Section II presents the design and mechanical implementation of the passive gripper. Section III describes full-state trajectory optimization in SE(3). Section IV reports validation and experiments, and Section V concludes the paper.

II. SPARO: Passive Gripper Design

SPARO is designed to be simple, light, and low-cost. It has two parts: one that closes the claws using impact energy, and another that opens the claws by turning the robot's body. The design is platform-agnostic, meaning that any host robot capable of generating a yaw (or, if needed, pitch/roll) rotation can operate the opening mechanism without dedicated end-effector actuation or sensing. The gripper is 3D printed using PET-G material, with only metal fasteners and spacers, resulting in a total weight of 290 g. The use of standard materials and a minimal number of components makes SPARO both cost-effective and easy to manufacture.

SPARO uses eight claws, inspired by [12], that curve inward and are paired opposite each other, as shown in Fig. 2a. Each claw has an activation protrusion (highlighted red in Fig. 2a) that defines the activation surface $\mathcal{A} = \bigcup_i \mathcal{A}_i$. Closure is guaranteed if a contact force F_{ext} is applied on any activation protrusion $\mathcal{A}_i$. The gripper has two stable states, open and closed, which makes it easier to control when it should grab or release. When closed, the tips of the claws fit together tightly, so they can hold thin objects like cables firmly. Parts of SPARO are shown in Fig. 2b.

A. Closure mechanism

The gripper closes by impact, utilizing springs that store energy when open and release it when they come into contact with an object. The activation surface is highlighted in green in Fig. 2a. When any protrusion is touched, the claws move inward along curved paths, holding the object from the sides and pulling it closer to the palm. This helps when the object is slightly off position or angle.

We evaluated configurations with one, two, and three springs. Adding springs increased the closure force and holding strength, but also increased stress on the 3D-printed components. Three springs offered the best trade-off, delivering a robust grasp without damaging SPARO. Each spring has a stiffness of $k_s = 250$ N/m. The claws lock fully when closed, providing a strong grip even on smaller objects, such as cables, which is important for long missions where saving energy matters. Objects larger than 15 cm in diameter may not trigger the closing properly or could cause the claws to become misaligned, however, this limit can be adjusted by scaling the gripper size.

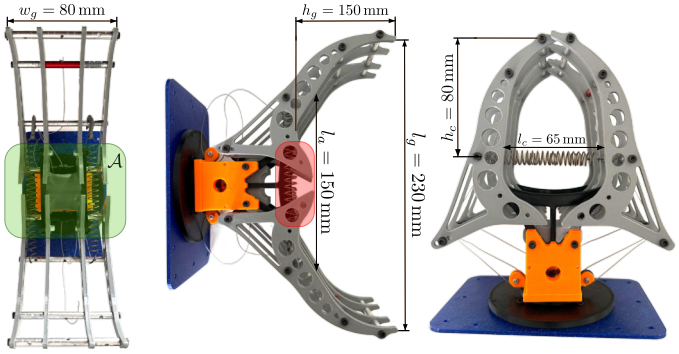

(a) SPARO with dimensional annotations. The activation surface $\mathcal{A}$ and protrusions are highlighted in green and red, respectively.

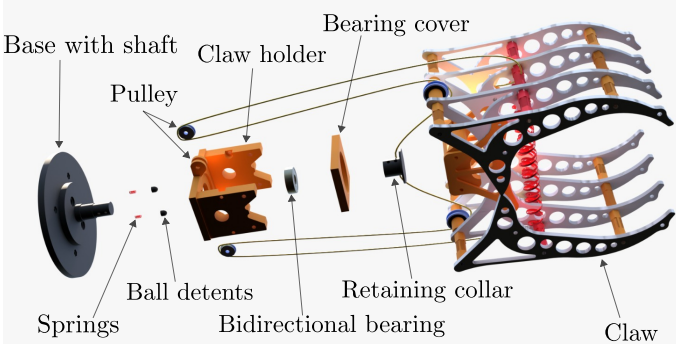

(b) Exploded view of mechanical components.

Fig. 2: Design overview of the SPARO.

B. Opening mechanism

The SPARO mechanism consists of a base with a shaft rigidly mounted to the vehicle, which is connected to the inner bearing ring. The outer ring of the bearing supports the claw holder, which is free to rotate relative to the robot. A cable is routed axially through the shaft and wrapped around it to form a spool. As the robot rotates, the shaft turns with it, winding the cable and pulling it tight. This traction opens the claws. A simple pulley system integrated into the claw holder introduces a mechanical advantage of approximately $\mu \approx 2$, effectively halving the torque required for actuation in exchange for doubling the rotation needed for a full opening. A retaining collar at the end of the shaft prevents unintentional cable unwinding.

Because the claw holder is mounted to the outer bearing ring, it is mechanically isolated from the vehicle frame and can rotate freely. This enables the robot body to rotate while the gripper remains stationary, but its orientation cannot be directly controlled. To ensure it resets to

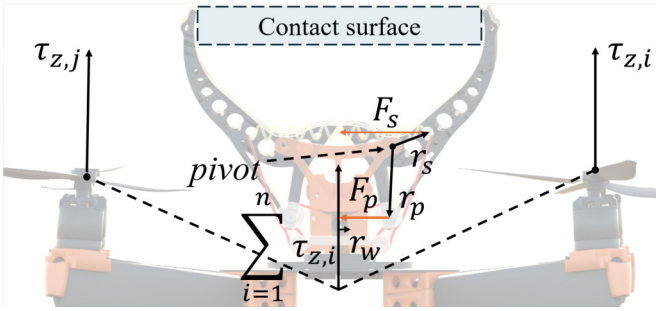

Fig. 3: Showing the relationship between the quadrotor actuation torques and the spring force.

a known configuration, spring-loaded ball detents are embedded in the fixed base. As the claw holder rotates, the detents engage with notches on the holder, passively indexing it to a predefined angular position and ensuring the gripper is correctly aligned for the next grasp.

To open the gripper with a quadrotor, we consider the relationship between the quadrotor actuation torques $\sum_i \boldsymbol{\tau}_{z,i}$ and the spring force $\mathbf{F}_s$ depicted in Fig. 3. The analysis is performed by balancing the moments around the pivot point. The spring exerts a force $\mathbf{F}_s$ at radius $\mathbf{r}_s$, producing a restoring moment. In parallel, a pulley transmits a pulling force $\mathbf{F}_p$ at radius $\mathbf{r}_p$. Considering the pulley's mechanical advantage μ, we can write the static equilibrium of moments about the pivot point:

$$\mathbf{r}_s \times \mathbf{F}_s = \mu\, \mathbf{r}_p \times \mathbf{F}_p. \tag{1}$$

Next, this pulling force from both sides is applied to a winding shaft of radius $\mathbf{r}_w$, generating a torque equal to the sum of the torques generated by all individual rotors:

$$2 \cdot \mathbf{r}_p \times \mathbf{F}_p = \sum_i \boldsymbol{\tau}_{z,i}. \tag{2}$$

The proposed design provides enough mechanical advantage to open the gripper by rotating the quadrotor. During opening, SPARO's claws must stay in contact with the perching surface to anchor the body. This contact prevents the mechanism from rotating as a whole and allows cable tension to build.

The gripper has two states and one transient state, as shown in Fig. 4, together with three transitions:

a) Closing: The closing action transitions the gripper from open to closed state, enabling the aerial manipulator to perch.

b) Opening: A constant yaw rotation winds the cable and opens the gripper. To detect when the gripper is fully open, the yaw angle must remain unchanged for a duration t_d. The opening time t_o is recorded at this point.

c) Unwinding: A reverse yaw is applied for $t_r = t_o$ to unwind the cable and release tension, ensuring the gripper remains in the open state.

The gripper design has a bistable geometry, where both open and closed states are stable without requiring energy to maintain the configuration. This feature conserves energy during prolonged mission times.

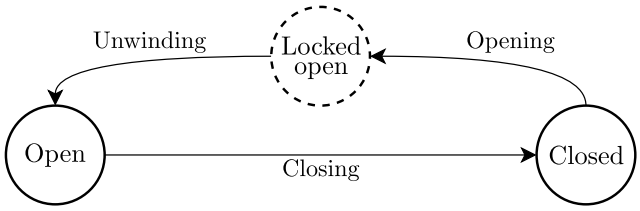

Fig. 4: SPARO gripper operation state machine.

III. Gripper-Aware Trajectory Optimization

We create the quadrotor's trajectory from start to goal by solving a single nonlinear optimization problem. This method optimizes the quadrotor's full state at every point, including position $\mathbf{p} \in \mathbb{R}^3$, quaternion orientation $\mathbf{q} \in \mathbb{R}^4$, linear velocity $\dot{\mathbf{p}} \in \mathbb{R}^3$, angular velocity $\boldsymbol{\omega} \in \mathbb{R}^3$, and linear acceleration $\ddot{\mathbf{p}} \in \mathbb{R}^3$. The 16-dimensional state vector is defined as

$$\mathbf{x}(t) = \left[\mathbf{p}^T(t)\ \ \mathbf{q}^T(t)\ \ \dot{\mathbf{p}}^T(t)\ \ \boldsymbol{\omega}^T(t)\ \ \ddot{\mathbf{p}}^T(t)\right]^T \in \mathbb{R}^{16}. \tag{3}$$

A first-order approximation thrust-based rigid-body model is used, requiring only the mass m, as in [19]. Translational motion is driven by the thrust force f and gravitational acceleration $\bar{g}$, while rotational motion is governed by the quadrotor's body rates $\boldsymbol{\omega}$ and orientation matrix $\mathbf{R} \in \mathrm{SO}(3)$. This minimal model allows the method to be applied directly to off-the-shelf quadrotors, requiring only basic parameters such as mass and dynamics constraints. The dynamics are expressed as

$$\begin{cases} \ddot{\mathbf{p}} = \dfrac{f}{m}\mathbf{R}\mathbf{e}_3 - \bar{g}\mathbf{e}_3, \\ \dot{\mathbf{R}} = \mathbf{R}\hat{\boldsymbol{\omega}}, \end{cases} \tag{4}$$

where $\mathbf{e}_3$ is the third column of the identity matrix, and $\hat{\boldsymbol{\omega}}$ denotes the skew-symmetric matrix representation of the cross product.

The NLP optimization problem that generates the full-state trajectory is defined as:

$$\min_{\mathbf{x}(t),T} \int_0^T \Big(\mathbf{w}\|\mathbf{x}(t)\|^2 + J_{\text{vert}}(t) + J_{\text{cone}}(t)\Big)dt + \sigma T \tag{5}$$

$$\forall t \in [0,T] \quad \text{s.t.} \quad 0 < T \le T_{\max},$$

$$\dot{\mathbf{x}}(t) = \mathbf{f}(\mathbf{x}(t),\, \mathbf{u}(t)),\ \ \mathbf{x}(0) = \mathbf{x}_{\text{i}},\ \ \mathbf{x}(T) = \mathbf{x}_{\text{g}}, \tag{6}$$

$$\|\dot{\mathbf{p}}(t)\|, \|\ddot{\mathbf{p}}(t)\|, \|\boldsymbol{\omega}(t)\| \le v_{\max}, a_{\max}, \boldsymbol{\omega}_{\max}, \tag{7}$$

$$\tau_{\min} \le \|\tau(t)\| \le \tau_{\max}, \tag{8}$$

$$\|\mathbf{p}(t) - \mathbf{p}_{\text{obs}}\|^2 \ge (r_{\text{obs}} + \delta)^2. \tag{9}$$

The initial state assumes hovering ($\dot{\mathbf{p}}(0) = \ddot{\mathbf{p}}(0) = 0$). The system dynamics are enforced by (6), and the physical limits on velocity, acceleration, and thrust are enforced by (7)-(8). The maximum trajectory duration $T_{\max}$ is estimated based on the Euclidean distance to the target and a nominal velocity of 0.5 m/s, which is always in constraint range. To avoid collisions during the approach, obstacle avoidance is enforced with constraint (9).

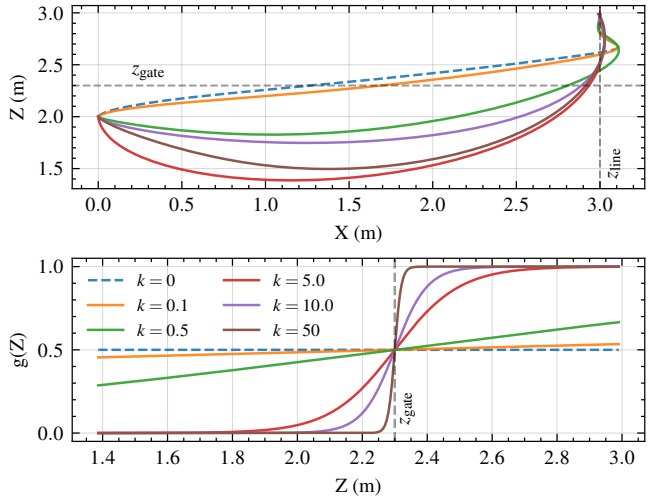

Fig. 5: Influence of gate sharpness κ on trajectory shaping. Top: Resulting trajectories for different κ values. Bottom: Gate function $g(z)$ profiles corresponding to each κ.

The optimization minimizes a cost function (5) that balances three key aspects: smoothness of the motion, aggressiveness, and vertical J_{vert} and cone J_{cone} guidance costs which encourage an approach from below the anchor point $\mathbf{p}_{\text{anch}}$. The relative importance of each state component is determined by the weighting matrix $\mathbf{w}$, and the time penalty is scaled by σ.

The tip of the gripper is defined as:

$$\mathbf{p}^G = \mathbf{p} + \mathbf{R}\mathbf{r}_{\text{tip}}, \tag{10}$$

where $\mathbf{r}_{\text{tip}}$ is distance from base frame to gripper tip. The lateral distance ρ from the gripper tip $\mathbf{p}^G$ to the anchor point $\mathbf{p}_{\text{anch}}$ is defined as:

$$\rho(t) = \|\mathbf{p}^G_{xy}(t) - \mathbf{p}_{\text{anch},xy}\|. \tag{11}$$

To enable smooth, continuous transitions between the vertical and cone guidance costs, preserving differentiability, we define a smooth gate function in a generalized form:

$$g(\tau) = \frac{1}{2}\left(1 + \tanh\left(\kappa(\tau - \tau_{\text{gate}})\right)\right), \tag{12}$$

where κ determines the sharpness of the transition. The gate transitions smoothly from 0 to 1 as the quadrotor surpasses τ_{gate}.

A vertical ascent toward the anchor point is encouraged once the quadrotor's tip rises above a designated height gate z_{gate}. The reference target point is defined with the vertical line $\mathbf{p}_{\text{line}}(t) = \begin{bmatrix} p_{\text{anch},x} & p_{\text{anch},y} & z_{\text{line}}(t) \end{bmatrix}^T$ directly under the anchor with:

$$z_{\text{line}}(t) = z_{\text{gate}}(1 - \frac{t}{T}) + p_{\text{anch},z}\frac{t}{T}. \tag{13}$$

The effect of the gate sharpness parameter κ is shown in Fig. 5. Larger κ values enforce stricter convergence of the quadrotor to the vertical reference line z_{line} after passing z_{gate}, as observed when comparing $\kappa = 10$ and $\kappa = 50$. Lower values reduce this enforcement, allowing

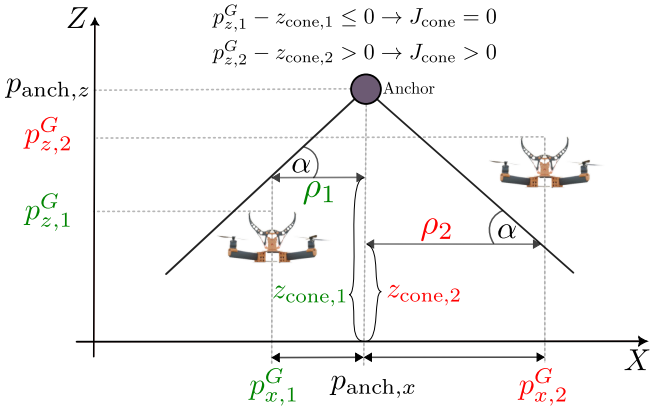

Fig. 6: Illustration of cost function J_{cone}, Eq. (16), in x-z plane. The green example yields zero cost as the gripper is inside the cone, unlike the red example, where the cone region is violated.

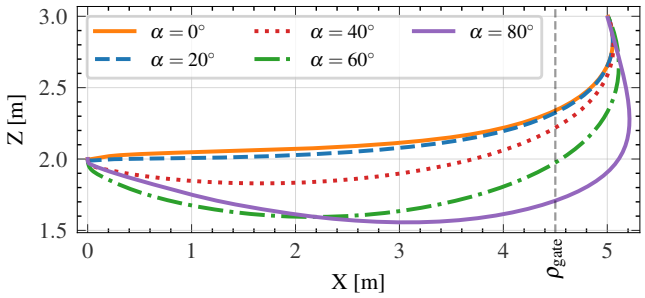

Fig. 7: The parameter α adjusts the shape of the approach from below. Higher values of α enforce steeper trajectories under the anchor.

the trajectory to deviate further from z_{line} and potentially overshoot it.

The corresponding vertical shaping cost is:

$$J_{\text{vert}}(t) = \lambda_{\text{vert}} \cdot g(p^G_z(t)) \cdot \left(\mathbf{p}^G(t) - \mathbf{p}_{\text{line}}(t)\right)^2. \tag{14}$$

This cost encourages the quadrotor to track a vertical line under the anchor, but only when the gate is active. The parameter λ_{vert} weight the penalization of J_{vert}.

To approach the anchor point from below, we define the cone whose tip is at the anchor point. The idea is that the quadrotor, i.e., the tip of the gripper, is forced to stay in that cone when it passes the lateral gate ρ_{gate}. The illustration of the cost is shown in Fig. 6. The cone height at lateral distance $\rho(t)$ is defined as:

$$z_{\text{cone}}(t) = p_{\text{anch,z}} - \tan(\alpha)\,\rho(t), \tag{15}$$

where α is the cone opening angle shown in Fig. 6. As seen in Fig. 7, increasing the α enforces a steeper approach from below sooner, while a smaller α permits a shallower path.

The gripper's shape also constrains the cone angle α. If α is too small, the trajectory may approach too shallowly, increasing the risk of lateral impact between the gripper and the anchor. To ensure safety, we define a minimum

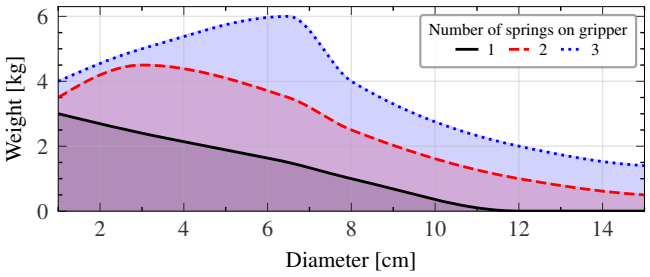

(a) Circular targets.

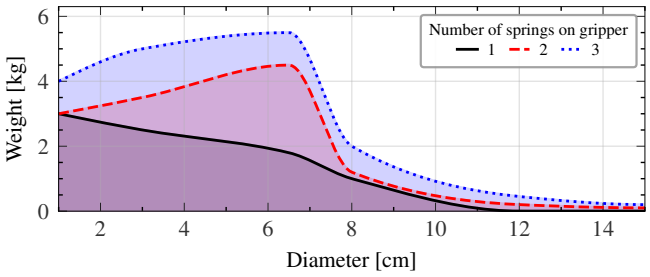

(b) Square targets mapped to outer diameter.

Fig. 8: SPARO payload capacity across different object sizes and shapes.

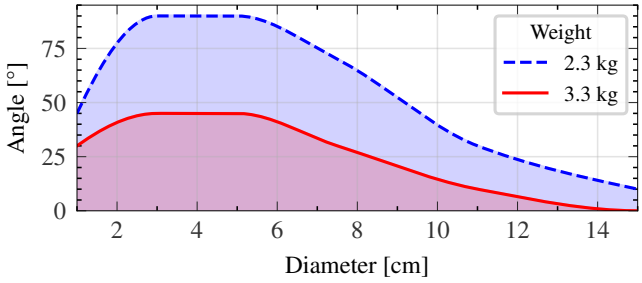

Fig. 9: Perching success map as a function of contact diameter and angle, evaluated for two configurations: quadrotor without payload and with 1 kg payload.

angle $\alpha_{\min} = 90° - \tan^{-1}(l_g/2h_g)$ based on the gripper's length l_g and height h_g, which yields 52° in our case.

The cone shaping cost is defined as:

$$J_{\text{cone}}(t) = \lambda_{\text{cone}} \cdot g(\rho(t)) \cdot \left(\left[p_z^G(t) - z_{\text{cone}}(t) \right]_+ \right)^2, \quad (16)$$

where $[\cdot]_+ = \max(\cdot, 0)$ and λ_{cone} is cost weight. This cost encourages the quadrotor to approach from below with reduced lateral velocity, thereby improving alignment with the surface and supporting passive closure.

The trajectory optimization is performed using the CasADi framework and the IPOPT solver, typically converging within 1000 iterations. Since perching is performed on known, fixed targets, real-time planning was not a requirement in this work. Nonetheless, the full trajectory is computed in under 5 s, and all computation is performed onboard the quadrotor. The resulting trajectory is time-sampled and streamed to the onboard controller at 100 Hz, enabling fully autonomous execution.

IV. Results and Validation

This section validates the SPARO as a passive gripper and the perching system. Gripper experiments evaluate closing, opening, geometric tolerance, and universality (mounting on different faces and platforms), while perching experiments evaluate end-to-end perching with the optimized trajectories on common materials such as aluminum, steel, and wood. All tests were performed with the plain PET-G printed gripper without any auxiliary adhesion, microspines, surface coatings, or inserts, thus representing a conservative, worst-case surface condition.

A. SPARO performance validation

Table I compares the SPARO gripper with existing aerial perching grippers, highlighting weight, actuation, payload, forces, and target size, with an emphasis on fully passive operation. The 290 g SPARO is fully 3D-printed, requires no electronics at the end-effector, reliably snap-closes upon contact, withstands over 500 cycles, achieves up to 6 kg payload with three springs, and successfully perches on cables, branches, and poles over a wide range of approach angles. Contact with the activation surface $\mathcal{A}$ (Section II) passively triggers snap closure. When closed, the claws interlock securely, enabling perching on thin cables. Targets with a diameter above 15 cm lie outside the guaranteed activation range. Over 500 closure cycles were performed without damage to the printed parts or springs. No fractures or permanent bends were seen during routine use.

We have tested configurations with one to three springs, while four springs caused damage to the gripper construction and were excluded. Payload capacity versus target diameter is shown in Figs. 8a and 8b for circular and square targets. Single-spring configurations performed poorly, while three springs achieved the best results with a maximum payload of 6 kg. Near a 6.5 cm diameter, closure is limited and interlocking fails, causing slipping or side forces. Targets above 15 cm mostly failed to trigger closure.

Forces were measured with an OnRobot HEX-E sensor. The peak closure force was 7 N, which serves as a reference for potential integration of adhesion or barbed contact surfaces. The activation force required on $\mathcal{A}$ was 9 N, indicating that strong impacts are not necessary to initiate closure, which is a key property that reduces the risk of damaging the gripper.

Figure 9 maps successful perching by target diameter, approach angle, and suspended mass. With a total system weight of 2.3 kg (quadrotor, gripper, battery), the SPARO perches on thin cables at approach angles up to 90°. At the worst-case load of 3.3 kg (including 1 kg payload, which is the maximum for the quadrotor we used), the allowed approach angle was reduced to about 42°.

The SPARO worked on different quadrotors and mounting positions and perched on varied surfaces like tree branches, PVC, and metal poles as seen in Fig. 10.

Fig. 10: SPARO's modality and universality across different robots and mounting configurations. The same gripper enables successful perching on various platforms, confirming ease of integration and repeatability.

B. End-to-End Autonomous Perching

End-to-end perching was validated by flying the optimized trajectories, closing the gripper on the target point, and then opening it. The experiments used a commercial Hexoon EDU-V2 quadrotor (weighing 2.09 kg with battery), equipped with an onboard Intel NUC 11TNHi5 and a Cube Orange+ flight controller unit. All planning and control ran on the onboard CPU. For visualization purposes and without loss of generality, the trajectories are shown in the x-z plane, where pitch dynamics dominate. However, both the trajectory planner and the quadrotor operate in full SE(3) and are capable of executing fully three-dimensional maneuvers.

An example flight is shown in Fig. 11, where the quadrotor closely tracks both position and body-rate commands. Small steady-state errors occurred but were acceptable because the activation surface $\mathcal{A}$ and the approach below make the contact reliable. The same maneuver was repeated multiple times with consistent success: the perching was successful each time the activation zone touched the anchor point.

After perching, the gripper must open to allow the quadrotor to detach and prepare for a new perch. The yaw-driven opening method from Section II-B is used, measuring the yaw angle on the onboard IMU. Although spring-loaded detents help realign the gripper after opening, they are not strong enough to resist rotation during the yaw maneuver. The pulley mechanism reduced the required yaw torque from 0.74 Nm to 0.37 Nm, which is consistent with expectations. Minor deviations are attributed to cable friction, bearing losses, and detent preload. Figure 12 shows the commanded and measured yaw during the opening and unwinding transitions, while the quadrotor is hovering. The accompanying time-lapse illustrates how the gripper remains stationary against the

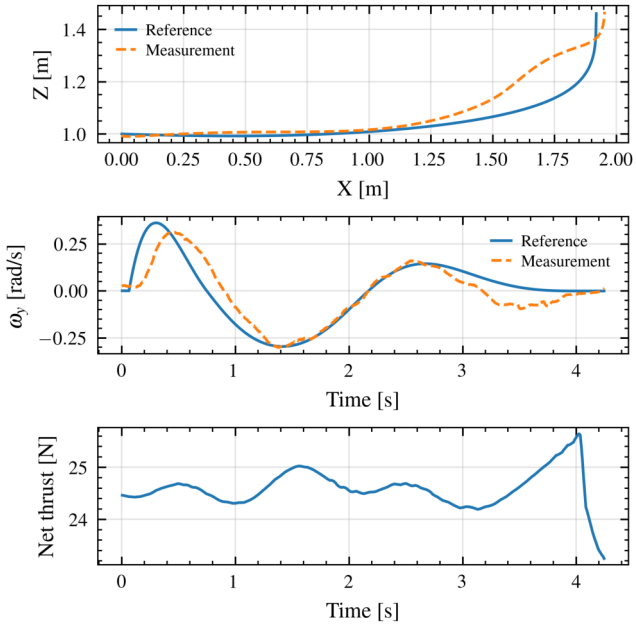

(a) Reference, measured position, yaw rate, and thrust.

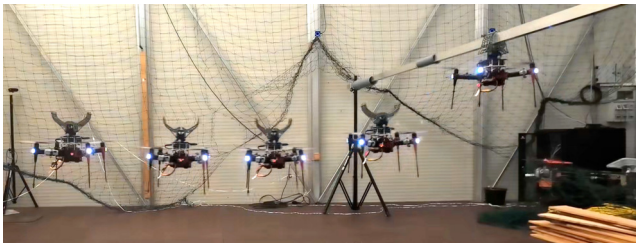

(b) Time-lapse of a full perching maneuver.

Fig. 11: Trajectory execution and control response.

surface while the quadrotor rotates, gradually opening the claws through mechanical coupling. Due to the inward-curving claws, the quadrotor descends slightly during opening, reducing the likelihood of accidental closure.

V. Conclusion

This paper presents SPARO, a passive, mechanically intelligent perching system that combines a snap-activated gripper with trajectory optimization to enable repeatable autonomous aerial perching. SPARO requires no onboard actuation or sensing and is opened using the host robot's rotational motion. Trajectories are generated using a holistic NLP that accounts for the gripper's passive dynamics and includes shaping costs to promote successful perching. The fully passive design reduces the overall gripper weight, allowing operation even on smaller-sized quadrotors. The extensive experiments showed the durability and effectiveness of such a gripper, allowing the aerial manipulators of multiple sizes to perch on various surfaces without reaching the mechanical breaking point. Future work will focus on extending the approach to more complex environments, incorporating perception-aware planning, and exploring advanced contact mechanics, including passive surface compliance and soft grippers.

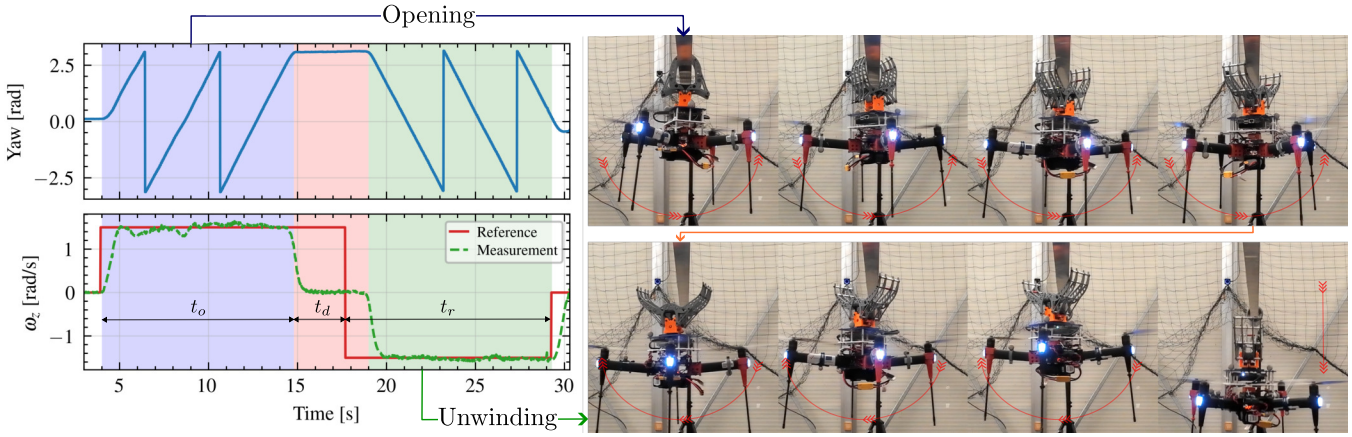

Fig. 12: Opening and unwind sequence. The left plot shows the yaw rates and yaw during the maneuver. The right time-lapse illustrates the robot rotating while the gripper remains fixed against the perching surface.

References

[1] B. Arbanas, A. Ivanovic, M. Car, M. Orsag, T. Petrovic, and S. Bogdan, "Decentralized planning and control for uav–ugv cooperative teams," *Autonomous Robots*, vol. 42, no. 8, pp. 1601–1618, 2018.

[2] J. Domislovic, M. Kozlik, V. Horvat, F. Petric, and M. Orsag, "Perch-and-tether strategy for extending ad hoc networks in communication-denied cbrne scenarios," in *2025 IEEE International Symposium on Safety Security Rescue Robotics (SSRR)*, pp. 184–189, 2025.

[3] S. Zhang and J. Liu, "Analysis and optimization of multiple unmanned aerial vehicle-assisted communications in post-disaster areas," *IEEE Transactions on Vehicular Technology*, vol. 67, no. 12, pp. 12049–12060, 2018.

[4] H. Hsiao, J. Sun, H. Zhang, and J. Zhao, "A mechanically intelligent and passive gripper for aerial perching and grasping," *IEEE/ASME Transactions on Mechatronics*, vol. 27, no. 6, pp. 5243–5253, 2022.

[5] H. Zhang, E. Lerner, B. Cheng, and J. Zhao, "Compliant bistable grippers enable passive perching for micro aerial vehicles," *IEEE/ASME Transactions on Mechatronics*, vol. 26, no. 5, pp. 2316–2326, 2021.

[6] T. G. Chen, K. A. Hoffmann, J. E. Low, K. Nagami, D. Lentink, and M. R. Cutkosky, "Aerial grasping and the velocity sufficiency region," *IEEE Robotics and Automation Letters*, vol. 7, no. 4, pp. 10009–10016, 2022.

[7] S. Lin, A. Lynch, and M. Liarokapis, "An ultra-light, ultra-fast, passive closing aerial gripping system capable of grasping, perching, and aerial manipulation," in *2024 IEEE International Symposium on Safety Security Rescue Robotics (SSRR)*, pp. 12–17, 2024.

[8] A. McLaren, Z. Fitzgerald, G. Gao, and M. Liarokapis, "A passive closing, tendon driven, adaptive robot hand for ultra-fast, aerial grasping and perching," in *2019 IEEE/RSJ International Conference on Intelligent Robots and Systems (IROS)*, pp. 5602–5607, 2019.

[9] A. Firouzeh, J. Lee, H. Yang, D. Lee, and K.-J. Cho, "Perching and grasping using a passive dynamic bioinspired gripper," *IEEE Transactions on Robotics*, vol. 40, pp. 213–225, 2024.

[10] W. Crooks, S. Rozen-Levy, B. Trimmer, C. Rogers, and W. Messner, "Passive gripper inspired by manduca sexta and the fin ray® effect," *International Journal of Advanced Robotic Systems*, vol. 14, no. 4, p. 1729881417721155, 2017.

[11] T. Kominami and K. Shimonomura, "Versatile perching using a passive mechanism with under actuated fingers for multirotor aav," *IEEE Robotics and Automation Letters*, vol. 9, no. 12, pp. 11226–11233, 2024.

[12] R. Zufferey, J. Tormo-Barbero, D. Feliu-Talegon, S. R. Nekoo, J. A. Acosta, and A. Ollero, "How ornithopters can perch autonomously on a branch," *Nature Communications*, vol. 13, Dec. 2022.

[13] L. Zheng and S. Hamaza, "Albero: Agile landing on branches for environmental robotics operations," *IEEE Robotics and Automation Letters*, vol. 9, no. 3, pp. 2845–2852, 2024.

[14] Y. Mikawa, N. Takesue, H. Mochiyama, M. Hassan, and K. Suzuki, "Snap gripper: Flexible mechanisms for flapping robot gripping, jumping, and landing," in *2025 IEEE 8th International Conference on Soft Robotics (RoboSoft)*, pp. 1–6, 2025.

[15] K. Nagaoka, H. Minote, K. Maruya, Y. Shirai, K. Yoshida, T. Hakamada, H. Sawada, and T. Kubota, "Passive spine gripper for free-climbing robot in extreme terrain," *IEEE Robotics and Automation Letters*, vol. 3, no. 3, pp. 1765–1770, 2018.

[16] T. Lan, L. Romanello, M. Kovac, S. F. Armanini, and B. Bahadir Kocer, "Aerial tensile perching and disentangling mechanism for long-term environmental monitoring," in *2024 IEEE International Conference on Robotics and Automation (ICRA)*, pp. 3827–3833, 2024.

[17] M. Askari, M. Benciolini, H.-V. Phan, W. Stewart, A. J. Ijspeert, and D. Floreano, "Crash-perching on vertical poles with a hugging-wing robot," *Communications Engineering*, vol. 3, no. 1, p. 98, 2024.

[18] P. Zheng, F. Xiao, P. H. Nguyen, A. T. Farinha, and M. Kovač, "Metamorphic aerial robot capable of mid-air shape morphing for rapid perching," *Scientific Reports*, vol. 13, 2023.

[19] M. W. Mueller, M. Hehn, and R. D'Andrea, "A computationally efficient motion primitive for quadrocopter trajectory generation," *IEEE Transactions on Robotics*, vol. 31, no. 6, pp. 1294–1310, 2015.

[20] Z. Wang, X. Zhou, C. Xu, and F. Gao, "Geometrically constrained trajectory optimization for multicopters," *IEEE Transactions on Robotics*, vol. 38, no. 5, pp. 3259–3278, 2022.

[21] J. Kim, M. C. Lesak, D. Taylor, D. J. Gonzalez, and C. M. Korpela, "Autonomous quadrotor landing on inclined surfaces using perception-guided active asymmetric skids," *IEEE Robotics and Automation Letters*, vol. 6, no. 4, pp. 7877–7877, 2021.

[22] K. Hang, X. Lyu, H. Song, J. A. Stork, A. M. Dollar, D. Kragic, and F. Zhang, "Perching and resting—A paradigm for UAV maneuvering with modularized landing gears," *Science Robotics*, vol. 4, no. 28, 2019.

[23] J. Ji, T. Yang, C. Xu, and F. Gao, "Real-time trajectory planning for aerial perching," in *2022 IEEE/RSJ International Conference on Intelligent Robots and Systems (IROS)*, pp. 10516–10522, 2022.

[24] J. L. Paneque, J. R. M.-d. Dios, A. Ollero, D. Hanover, S. Sun, A. Romero, and D. Scaramuzza, "Perception-aware perching on powerlines with multirotors," *IEEE Robotics and Automation Letters*, vol. 7, no. 2, pp. 3077–3084, 2022.

[25] Y. Gao, J. Ji, Q. Wang, R. Jin, Y. Lin, Z. Shang, Y. Cao, S. Shen, C. Xu, and F. Gao, "Adaptive tracking and perching for quadrotor in dynamic scenarios," *IEEE Transactions on Robotics*, vol. 40, pp. 499–519, 2024.